Title

Electronic structure and direct observation of ferrimagnetism in multiferroic hexagonal YbFeO3

Journal

Physical Review B, 95(22)

ISSN

2469-9950

Authors

Cao, Shi

Sinha, Kishan

Zhang, Xin

et al.

Publication Date

2017-06-01

DOI

10.1103/physrevb.95.224428

Peer reviewed

Electronic structure and direct observation of ferrimagnetism in multiferroic hexagonal $YbFeO_3$

Shi Cao,[1] Kishan Sinha,[1] Xin Zhang,[1] Xiaozhe Zhang,[2,1] Xiao Wang,[3] Yuewei Yin,[1] Alpha T. N'Diaye,[4] Jian Wang,[5] David J. Keavney,[6] Tula R. Paudel,[1] Yaohua Liu,[7] Xuemei Cheng,[3] Evgeny Y. Tsymbal,[1,8] Peter A. Dowben,[1,8] and Xiaoshan Xu[1,8,*]

[1]*Department of Physics and Astronomy, University of Nebraska, Lincoln, Nebraska 68588, USA*
[2]*Department of Physics, Xi'an Jiaotong University, Xi'an 710049, People's Republic of China*
[3]*Department of Physics, Bryn Mawr College, Bryn Mawr, Pennsylvania 19010, USA*
[4]*Advanced Light Source, Lawrence Berkeley National Laboratory, Berkeley, California 94720, USA*
[5]*Canadian Light Source, Saskatoon, SK, S7N 2V3 Canada*
[6]*Advanced Photon Source, Argonne National Laboratory, Argonne, Illinois 60439, USA*
[7]*Quantum Condensed Matter Division, Oak Ridge National Lab, Oak Ridge, Tennessee 37831, USA*
[8]*Nebraska Center for Materials and Nanoscience, University of Nebraska, Lincoln, Nebraska 68588, USA*

(Received 22 March 2017; revised manuscript received 21 May 2017; published 26 June 2017)

The magnetic interactions between rare-earth and Fe ions in hexagonal rare-earth ferrites (h-RFeO$_3$), may amplify the weak ferromagnetic moment on Fe, making these materials more appealing as multiferroics. To elucidate the interaction strength between the rare-earth and Fe ions as well as the magnetic moment of the rare-earth ions, element-specific magnetic characterization is needed. Using x-ray magnetic circular dichroism, we have studied the ferrimagnetism in h-$YbFeO_3$ by measuring the magnetization of Fe and Yb separately. The results directly show antialignment of magnetization of Yb and Fe ions in h-$YbFeO_3$ at low temperature, with an exchange field on Yb of about 17 kOe. The magnetic moment of Yb is about 1.6 μ_B at low temperature, significantly reduced compared with the 4.5 μ_B moment of a free Yb^{3+}. In addition, the saturation magnetization of Fe in h-$YbFeO_3$ has a sizable enhancement compared with that in h-$LuFeO_3$. These findings directly demonstrate that ferrimagnetic order exists in h-$YbFeO_3$; they also account for the enhancement of magnetization and the reduction of coercivity in h-$YbFeO_3$ compared with those in h-$LuFeO_3$ at low temperature, suggesting an important role for the rare-earth ions in tuning the multiferroic properties of h-RFeO$_3$.

DOI: 10.1103/PhysRevB.95.224428

I. INTRODUCTION

The diverse magnetic properties of rare-earth (RE) transition-metal (TM) oxides are due to the interplay between the distinct magnetism of rare-earth and transition-metal ions. For the transition-metal ions, the magnetic moments come from d electrons, which are well exposed to the local environment. In contrast, for rare-earth ions, the magnetic moments come from $4f$ electrons, which are close to the inner core and have significant contributions from both spin and orbital angular momentum [1]. While the stronger interaction between the transition-metal ions determines the framework of the magnetic order in RE-TM oxides [2–4], the weaker interaction between the rare-earth and transition-metal ions, on the other hand, generates interesting phenomena such as spin reorientation and moment compensation [5–11]. Despite the importance of the RE-TM interactions, a comprehensive understanding of its underpinnings and implications is still lacking for many material systems.

In this work, we study the magnetic interaction between rare-earth and transition-metal ions by measuring the magnetization of the rare-earth and transition-metal ions separately using an element-specific method. In particular, we study hexagonal $YbFeO_3$, a member of hexagonal rare-earth ferrites (h-RFeO$_3$, R = Ho-Lu, Y, and Sc). Hexagonal h-$YbFeO_3$ have a layered crystal structure in which both RE and Fe atoms adopt a two-dimensional triangular lattice, as shown in Fig. 1 [12]. Below about 1000 K, the h-$YbFeO_3$ crystal structure undergoes a distortion, corresponding to a rotation of the FeO_5 local structure and a buckling of the rare-earth layer, which induces improper ferroelectricity [13–17]. The rotation of FeO_5 also cants the moment on Fe, via the Dzyaloshinskii-Moriya interaction, generating weak ferromagnetism on top of a 120° antiferromagnetic order below about 120 K, as illustrated in Fig. 1 [18–20]. The spontaneous magnetization is along the c axis. Recent work demonstrated that a superlattice structure of hexagonal Lu-Fe-O materials is promising for realizing room-temperature multiferroic materials with coexisting ferroelectricity and ferromagnetism [21], a property that has potential application in energy-efficient information processing and storage [22].

In h-$YbFeO_3$, the Fe-Fe interaction is expected to dominate the framework of the magnetic ordering, as corroborated by the fact that the ordering temperature of h-$YbFeO_3$ is almost the same as that of h-$LuFeO_3$ (noting that Lu^{3+} is nonmagnetic) [16,17,23,24]. The Yb-Fe interaction is weaker but sufficient enough to partially align the moment on Yb and contribute to the total magnetization. Indeed, an enhancement of magnetization of h-$YbFeO_3$, compared with that in h-$LuFeO_3$, has been observed previously [23,24] to be up to about 3 μ_B/f.u. at 3 K, in contrast to 0.018 μ_B/f.u. in h-$LuFeO_3$ [13,16]. The Yb-Fe interaction could, in principle, align or antialign the moments of Fe and Yb. At the compensation temperature [3,5], the magnetization of Fe and Yb cancel, and an indication of this was observed previously at about 80 K [24]. On the

*Corresponding author: xiaoshan.xu@unl.edu

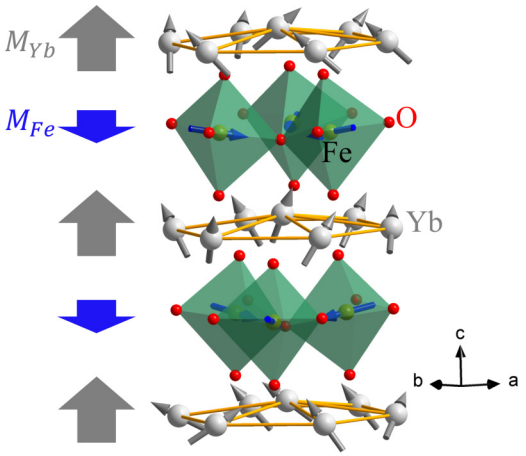

FIG. 1. The crystal structure of h-$YbFeO_3$ and a schematic of the magnetic structure. The arrows on the atoms indicate the atomic magnetic moments. M_{Fe} and M_{Yb} are the magnetization of Fe and Yb along the c axis, respectively, which are antialigned at low temperature. The Fe moments form a 120° antiferromagnetic order in the basal plane, with only a very small component along the c axis. The Yb moments are partially aligned by the Yb-Fe exchange field.

other hand, direct observation of antialignment between the Fe and Yb magnetization is still lacking. In addition, the previously reported large magnetization (about 3 μ_B/f.u.) [24] at low temperature is more consistent with a free Yb^{3+}, but unexpected when considering the effect of the crystal field generated by the local environment [25–29]. The crystal field could significantly change the effective magnetic moment and the magnetic anisotropy at low temperature [28,30].

To elucidate the Yb-Fe interaction and the magnetic moment of Yb, we have studied the electronic structure of h-$YbFeO_3$ using x-ray absorption spectroscopy (XAS) and x-ray photoemission spectroscopy (XPS), and we measured the magnetization of Fe and Yb separately using x-ray magnetic circular dichroism (XMCD). We have found a large exchange field (17 kOe) on Yb, while the magnetic moment of Yb is significantly reduced from the value of a free ion. The mixed valence of Yb was investigated and found only at the surface of samples grown in a reducing environment, suggesting a minimal effect on the magnetism of h-$YbFeO_3$.

II. METHODS

Hexagonal $YbFeO_3$ (001) films (20–50 nm) were deposited on yttrium-stabilized zirconia (YSZ) (111) substrates and on Fe_3O_4 (111)/Al_2O_3 (001) substrates using pulsed laser (248 nm) deposition in a 5 mtorr oxygen and argon environment, at 750 °C with a laser fluence of about 1 J cm^2 and a repetition rate of 2 Hz [13,14,31]. The film growth was monitored using reflection high-energy electron diffraction (RHEED). All the films studied with x-ray absorption spectroscopy and x-ray magnetic circular dichroism were grown in an oxygen environment. The crystal structures of the h-$YbFeO_3$ films were characterized by x-ray diffraction (XRD) using a Rigaku D/Max-B diffractometer, with Co $K\alpha$ radiation (1.7903 Å). The linear x-ray absorption spectroscopy on the Fe L and O K edges was studied using an x-ray photoemission electron microscope (X-PEEM) at the SM beamline of the Canadian Light Source with a linearly polarized x ray. The circular x-ray absorption (fluorescence) spectroscopy of Yb M and Fe L edge measurements was performed at the bend magnet beamline 6.3.1 in the Advanced Light Source at Lawrence Berkeley National Laboratory and at the beamline 4-ID-C in the Advanced Photon Source at Argonne National Laboratory, respectively. The angle-resolved x-ray photoemission spectra (ARXPS) were obtained using a SPECS PHOIBOS 150 energy analyzer. A nonmonochromatized Al $K\alpha$ x-ray source, with a photon energy 1486.6 eV, was used with various emission angles, as previously reported [32].

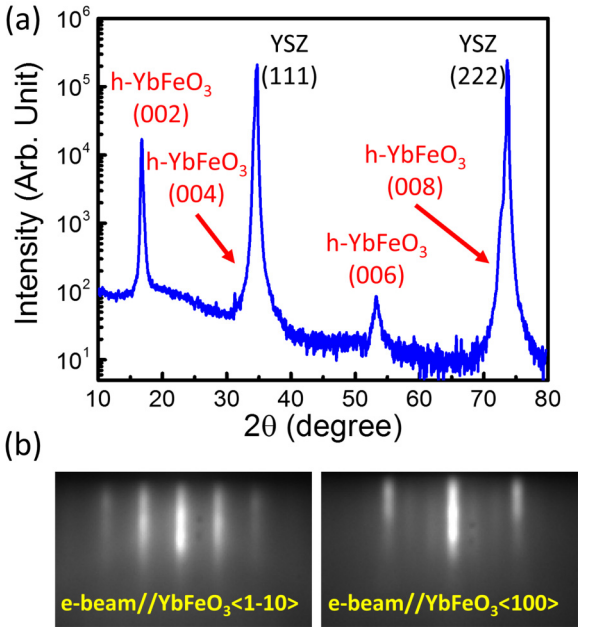

FIG. 2. (a) θ-2θ x-ray diffraction measurement of an h-$YbFeO_3$ film grown on yttrium-stabilized zirconia (YSZ). (b) RHEED patterns of an h-$YbFeO_3$ film with electron beam along the ⟨1-10⟩ and ⟨100⟩ directions.

III. RESULTS AND ANALYSIS

A. Crystal structure and local environment of Fe

To verify the structure and phases of the epitaxial films, we carried out x-ray diffraction, electron diffraction, and x-ray spectroscopy measurements. Figure 2(a) shows the x-ray diffraction (θ-2θ scan) of h-$YbFeO_3$/YSZ films. No additional peak other than those expected for h-$YbFeO_3$ and the substrate is visible in this large-range scan, indicating no impurity phases. As shown in Fig. 2(b), RHEED images show diffraction streaks consistent with a flat surface and the structure of h-$YbFeO_3$ [13,31].

The x-ray absorption spectra provided further confirmation of the local structure of Fe, from the Fe L edge spectra taken with a linearly polarized x ray. The local environment of Fe in h-$YbFeO_3$ is a trigonal bipyramid, with two apex O atoms (top and bottom) and three equator O atoms (in the Fe layer) as shown in Fig. 1 as well as in Fig. 3(a), inset. This structure makes the out-of-plane direction (along the c axis) and the in-plane direction (in the a-b plane) two distinct

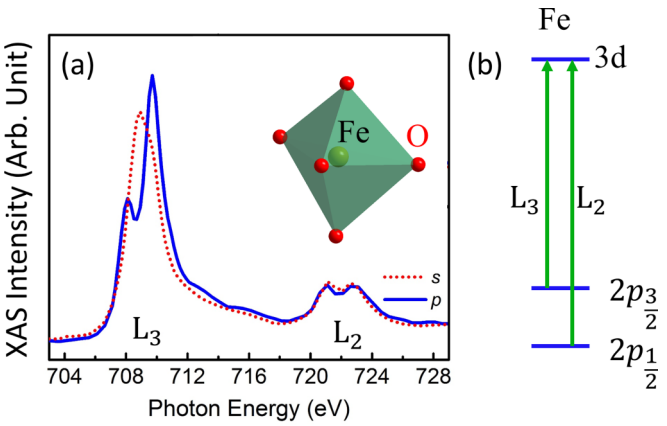

FIG. 3. (a) X-ray absorption spectra at the Fe L edge, measured using a linearly polarized x ray. Inset: the FeO_5 local environment. (b) Schematic illustration of the L_2 and L_3 excitation.

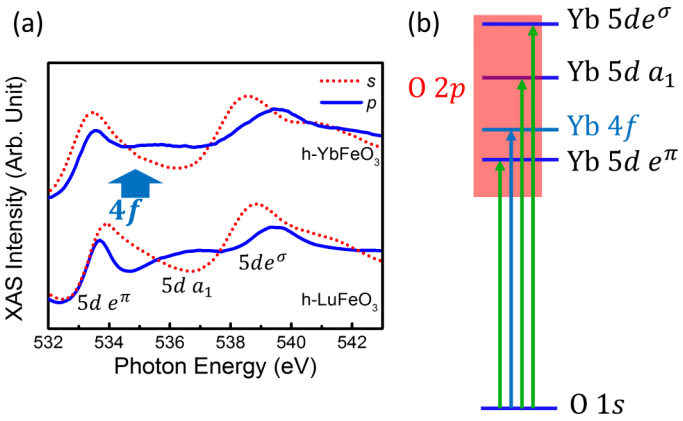

FIG. 4. (a) X-ray absorption spectra at the O K edge of h-$LuFeO_3$ and h-$YbFeO_3$, measured using linearly polarized x rays. The arrow indicates the $4f$ state. (b) Schematic illustration of the O K edge excitation and the hybridization between the O and Yb states.

crystalline directions. Using a linearly polarized x ray, we measured the absorption spectra at the Fe L edge, as illustrated in Fig. 3(b). As shown in Fig. 3(a), the spectrum with an s-polarized x ray (E vector in the a-b plane) and that with a p-polarized x ray (E vector along the c axis) show an obvious contrast, consistent with the large structural anisotropy. The spectra and linear dichroism in Fig. 3(a) match those observed previously for h-$LuFeO_3$ [20,21,33,34], confirming that the local environments of the FeO_5 moiety in the two materials are almost identical.

B. The electronic structure of Yb

While the electronic structure of Fe in h-$LuFeO_3$ and h-$YbFeO_3$ are superficially similar, the electronic structure of Yb^{3+} is expected to be different from that of Lu^{3+} by the presence of one fewer $4f$ electron. To probe the unoccupied states of Yb, we measured the excitation of electrons from O $1s$ states to O $2p$ states (O K edge) using an x ray. Nominally, O $2p$ states are fully occupied; the O $1s$ to O $2p$ excitation is forbidden by the Pauli exclusion principle. If, on the other hand, the O $2p$ states are hybridized with the Yb states, the O $2p$ states will be slightly unoccupied and give rise to observable O $1s$ to O $2p$ excitation; one can infer the energy of the unoccupied Yb states using the excitation energies [20]. As shown in Fig. 4(a), with linearly polarized x rays, several features can be observed in the absorption spectra. Previously, we carried out symmetry analysis of the absorption spectra measured on h-$LuFeO_3$ and identified the origin of these features mainly as the $5d$ orbitals, split in the crystal field: e^{π}, a_1, and e^{σ} [see Fig. 4(b)] [20]. Compared with the x-ray absorption spectra of h-$LuFeO_3$, the spectra of h-$YbFeO_3$ show additional density of states, as indicated in Fig. 4(a), which is expected to be the unoccupied $4f$ state that is hybridized with the O $2p$ states.

The $4f^{13}$ configuration of Yb can also be probed by measuring the excitation directly to the unoccupied $4f$ states (in the absence of s-f hybridization, none exist with Lu^{3+}). As shown in Fig. 5(a), x-ray absorption spectra at the Yb M edge were measured at 18 K. Two peaks are observed in the absorption spectra at approximately 1513 and 1555 eV, which can be assigned to M_5 (initial state $3d_{5/2}$) and M_4 (initial state $3d_{3/2}$) excitations, respectively, according to the photon energy [35] [see Fig. 5(b)]. The M_5 transition in Yb, which is allowed by the angular-momentum selection rule, can be described using the one-electron (hole) picture, without many-body interactions, due to the simple initial (full $3d_{5/2}$, one hole in $4f_{7/2}$) and final (one hole in $3d_{5/2}$, full $4f_{7/2}$) states, consistent with the observed sharp, structureless peak in Fig. 5(a). The M_4 excitation ($3d_{3/2}$ to $4f_{7/2}$), on the other hand, is not allowed by the angular-momentum selection rule. The nonzero intensity of the M_4 peak suggests that the crystal-field splitting and the Yb $4f$ O $2p$ hybridization reduce the symmetry of the electronic states considerably, which is in line with the observed contribution to the O K edge excitation by the Yb $4f$ state shown in Fig. 4(a).

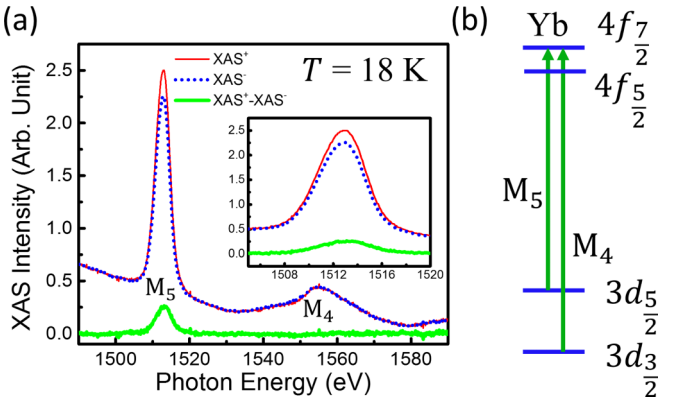

FIG. 5. (a) X-ray absorption spectra at the Yb M edge, measured using an x ray polarized counterclockwise. XAS^+ (XAS^-) is the spectrum measured in magnetic field along the $+z$ ($-z$) direction. (b) Schematic illustration of the Yb M edge excitation. The crystalline c axis of h-$YbFeO_3$ is along the z direction.

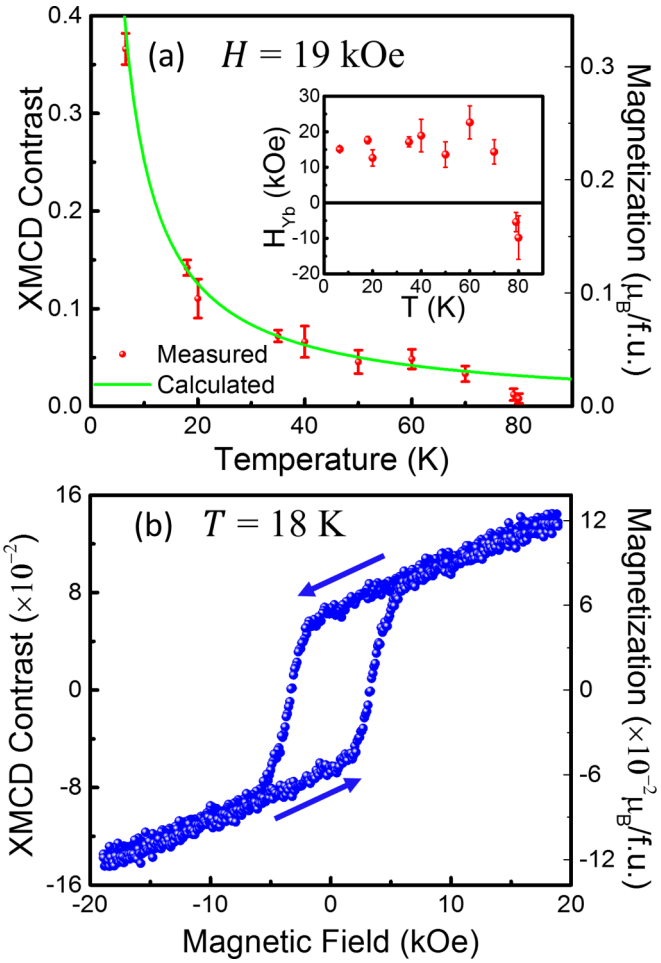

FIG. 6. XMCD contrast at the Yb M_5 edge and the corresponding magnetization. (a) Temperature dependence measured in a 19 kOe magnetic field; the line is calculated using the parameters analyzed from (b). Inset: H_{Yb} extracted from the mean-field theory (see text in Sec. IV B). (b) Magnetic-field dependence measured at 18 K. The magnetic field is along the c axis.

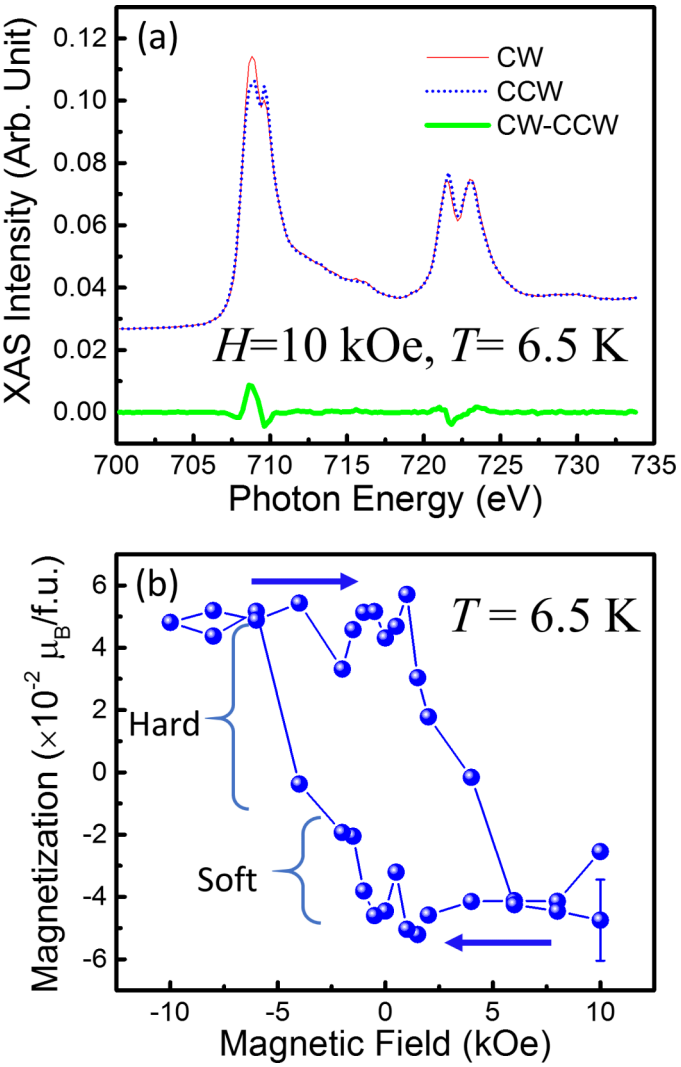

FIG. 7. (a) Absorption spectra at the Fe L edge measured with circularly polarized x rays in a 10 kOe field at 6.5 K. CW and CCW stand for clockwise and counterclockwise polarization of the x rays, respectively. (b) Magnetic-field dependence of the magnetization of Fe at 6.5 K, which contains a soft and a hard component (see the discussion in Sec. IV D). The magnetic field is along the c axis.

C. The ferrimagnetism of h-$YbFeO_3$

1. Magnetization of Yb and Fe

To study the magnetization of Yb, we carried out x-ray magnetic circular dichroism measurements by comparing the absorption spectra using a circularly polarized x ray in opposite magnetic fields. As shown in Fig. 5(a), the x-ray absorption spectra measured in 19 kOe and −19 kOe magnetic fields along the z direction show a clear contrast. We define the XMCD contrast as $\frac{2(I^+-I^-)}{I^++I^-}$, where I^+ and I^- are the M_5 peak areas of the absorption spectra in positive and negative magnetic fields, respectively.

The XMCD contrast measured at $H = 19$ kOe, for various temperatures between 6.5 and 80 K, is displayed in Fig. 6(a). The value of the XMCD signal decreases rapidly at low temperature, inconsistent with typical ferromagnetic dependence, which typically follows Bloch's law (i.e., a slow decrease at low temperature but much faster close to the magnetic ordering temperature) [36]. Figure 6(b) shows the field dependence of the XMCD contrast of Yb at 18 K. A clear hysteresis is observed with a coercive field of approximately 3.5 kOe. The magnetization converted from the XMCD contrast (see Appendix A) is also displayed in Fig. 6.

Figure 7(a) shows the spectra of x-ray absorption of the Fe L edge measured in a circularly polarized x ray in a 10 kOe magnetic field at 6.5 K. A clear difference is observed between the spectra measured using x rays of different polarizations, which can be used to estimate the magnetization of Fe [37]. Figure 7(b) shows the magnetic-field dependence of the Fe magnetization calculated from the XMCD contrast using the sum rule [37–39]. A hysteretic behavior is observed, with a coercive field of approximately 4 kOe, consistent with the value found in previous bulk magnetometry measurements [23,24]. This coercive fields is also similar to that of Yb in Fig. 6(b), indicative of the exchange field on Yb generated by Fe. The saturation magnetization of Fe is $0.05 \pm 0.01 \mu_B$/f.u., which corresponds to a small projection of the Fe moment

along the c axis. From Figs. 6 and 7, we find that the magnetization of Fe is antiparallel to the magnetic field and to that of the Yb magnetization at low temperature, as also illustrated in Fig. 1. This provides a direct observation of ferrimagnetic order in h-$YbFeO_3$.

2. The low-temperature magnetic moment of Yb

As shown in Fig. 6(b), the magnetization of Yb does not saturate in the measurement condition; instead, it shows a linear relation with a magnetic field when the field is much larger than the coercive field, which is consistent with a susceptibility behavior and somewhat akin to paramagnetism for Yb. We can, nonetheless, further analyze the magnetic moment on Yb using the mean-field theory [36], which has been extensively discussed historically in orthoferrites and garnets [10,11,40–43].

In the mean-field theory, the exchange interactions are modeled using the molecular fields. Assuming that the saturation magnetization of Fe is $M_{\mathrm{Fe,S}}$ (in μ_B/f.u.), the magnetization of Fe is given by

$$M_{\mathrm{Fe}} = M_{\mathrm{Fe,S}} L(x_{\mathrm{Fe}}), \tag{1}$$

where $L(x) = \coth(x) - \frac{1}{x}$ is the Langevin function, $x_{\mathrm{Fe}} = \frac{(\Gamma_{\mathrm{YbFe}} M_{\mathrm{Yb}} + \Gamma_{\mathrm{Fe}} M_{\mathrm{Fe}} + \mu_0 H) M_{\mathrm{Fe,S}}}{k_B T}$, M_{Yb} is the magnetization of Yb, Γ_{YbFe} and Γ_{Fe} are the molecular field parameters for the Yb-Fe and Fe-Fe interactions, respectively, μ_0 is the vacuum permittivity, k_B is the Boltzmann constant, H is the external magnetic field, and T is the temperature. The magnetization of Yb is given by

$$M_{\mathrm{Yb}} = \mu_{\mathrm{Yb}} L(x_{\mathrm{Yb}}), \tag{2}$$

where $x_{\mathrm{Yb}} = \frac{(\Gamma_{\mathrm{YbFe}} M_{\mathrm{Fe}} + \mu_0 H)\mu_{\mathrm{Yb}}}{k_B T}$, and μ_{Yb} is the magnetic moment of Yb. No Yb-Yb exchange interaction is included since such exchange interactions are too weak to play a role in the temperature range investigated in this work [3,5].

When the magnetic field is much larger than the coercive field and the temperature is much lower than the magnetic ordering temperature for the Fe ($\approx$120 K for h-$YbFeO_3$) [24], one may treat $|M_{\mathrm{Fe}}| \approx M_{\mathrm{Fe,S}}$ as a constant. As shown in Fig. 6(b), at $T = 18$ K, when H is between 6 and 19 kOe, the XMCD contrast shows a linear dependence with magnetic field, suggesting that x_{Yb} is small enough that the Langevin function takes a linear form with respect to the magnetic field H:

$$M_{\mathrm{Yb}} = \mu_{\mathrm{Yb}}^2 \frac{\Gamma_{\mathrm{YbFe}} M_{\mathrm{Fe}} + \mu_0 H}{3 k_B T}. \tag{3}$$

According to Eq. (3), the slope of the field dependence of M_{Yb} (susceptibility) is $\chi_{\mathrm{Yb}} = \frac{dM_{\mathrm{Yb}}}{dH} = \frac{\mu_{\mathrm{Yb}}^2 \mu_0}{3 k_B T}$, which leads to $\mu_{\mathrm{Yb}} = 1.6 \pm 0.1\ \mu_B$, a value much smaller than the magnetic moment of a free Yb (4.5 μ_B/f.u.) [44].

3. Exchange field on Yb

According to Eq. (3), the remanent magnetization (magnetization in zero H) is expected to be

$$M_{\mathrm{Yb},R} = \frac{\mu_{\mathrm{Yb}}^2 \Gamma_{\mathrm{YbFe}} M_{\mathrm{Fe}}}{3 k_B T}. \tag{4}$$

Because M_{Fe} and M_{Yb} have different signs in zero H [see Figs. 6(b) and 7(b)], one finds $\Gamma_{\mathrm{YbFe}} < 0$ from Eq. (4).

Using the value $M_{\mathrm{Yb},R} = 0.057\ \mu_B$/f.u. at 18 K from Fig. 6(b), one can calculate the exchange field on Yb: $H_{\mathrm{Yb}} = (\Gamma_{\mathrm{YbFe}} M_{\mathrm{Fe}})/\mu_0 = 17$ kOe. We also note that the exchange field on Yb generated by Fe in h-$YbFeO_3$ is about an order of magnitude larger than the value 1.6 kOe in orthorhombic $YbFeO_3$ and that in rare-earth orthoferrites in general [3]. This large difference may come from the dramatic differences between the bond lengths and bond angles in the hexagonal and orthorhombic $YbFeO_3$ structures.

D. The possible mixed valence of Yb

A mixed valence (Yb^{3+} and Yb^{2+}) may play a role in the magnetism of h-$YbFeO_3$ as well as the determination of the magnetization on the Yb^{3+}. In principle, there is a tendency to form Yb^{2+} due to the stability of the $4f^{14}$ configuration. Although it will not affect the XMCD method discussed above since Yb^{2+} does not contribute to the Yb M_5 x-ray absorption in the first place (the excitations to the fully occupied $4f$ states are forbidden in Yb^{2+}), it will be important for bulk magnetometry. We investigated the possibility of a mixed valence in h-$YbFeO_3$ using ARXPS by probing the core-level electronic structure.

Figure 8(a) shows the Fe $2p$ x-ray photoemission spectra for both h-$LuFeO_3$ and h-$YbFeO_3$. The good match between the Fe $2p_{3/2}$ peaks of h-$LuFeO_3$ and h-$YbFeO_3$ in Fig. 8(a) indicates that Fe core-level electronic structures are similar in these two ferrites. Previously, we have studied the x-ray photoemission spectra of Fe $2p$ using the Gupta and Sen (GS) multiplet fitting [45,46] of Fe $2p_{3/2}$ in h-$LuFeO_3$, and we concluded that the Fe $2p$ and its satellite peaks are characteristic of a nominal Fe^{3+} valence [32]. The same analysis applies here in h-$YbFeO_3$ as well. These features also do not vary with emission angle (data not shown). As a result, both the surface and the bulk part of the h-$YbFeO_3$ are in the nominal Fe^{3+} valence state.

We also did not find any indication of Yb^{2+} in the film samples grown in an oxygen environment (used for x-ray-absorption spectroscopy and x-ray magnetic circular dichroism in Figs. 2–7). To investigate the possible appearance of Yb^{2+}, we studied ARXPS on the h-$YbFeO_3$ films prepared in an argon environment. A comparison with two samples grown in oxygen and argon environments is displayed in Fig. 8(b). At the 0° takeoff angle (perpendicular to surface), the XPS spectra of Yb are identical for both h-$YbFeO_3$ samples. At the 70° takeoff angle, which probes mostly the surface [47,48], the XPS spectra of the sample grown in an oxygen environment (lower panel) do not show a clear difference from that at 0°, and the surface appears to be slightly Yb-rich. In contrast, for the sample grown in the argon environment, the XPS spectra at the 70° takeoff angle exhibit additional intensity at the $5p$ peak, indicating a Yb^{2+} valence [49]. The correlation between the growth conditions indicates that the presence of oxygen vacancy promotes the reduction of Yb^{3+} at the surface. Although slightly YbO-rich, the mixed surface termination (both iron oxide and YbO appear present at the surface) differs from the FeO termination seen for $LuFeO_3$ [32].

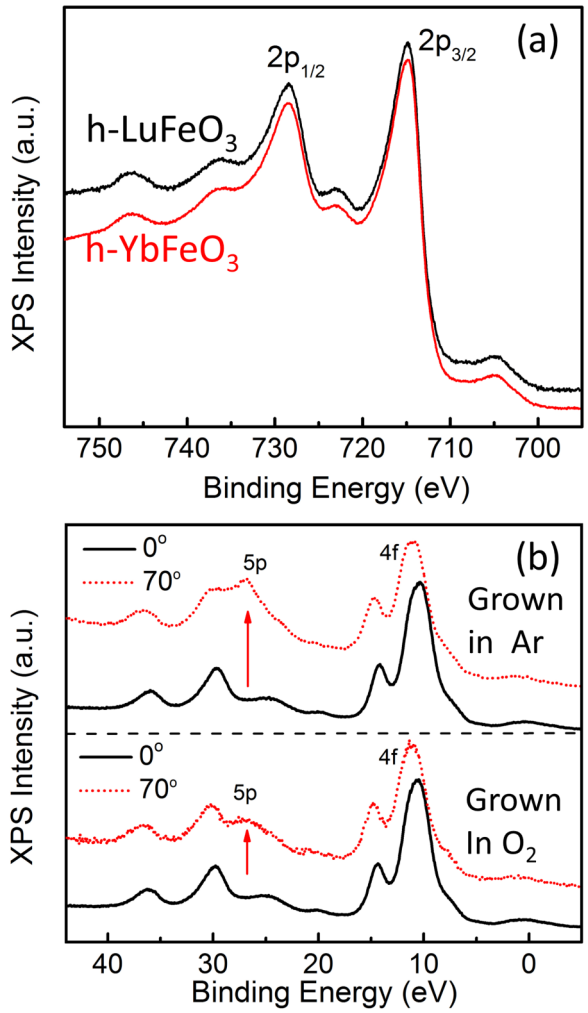

FIG. 8. (a) X-ray photoelectron spectra around the Fe $2p$ core level for h-$YbFeO_3$ and h-$LuFeO_3$. (b) The x-ray photoelectron spectra around the Yb $5p$ edge of h-$YbFeO_3$ film samples grown in an Ar and an O_2 environment measured at 0° and 70° take-off angle, corresponding to 2 and 0.7 nm probing depth, respectively [47,48].

IV. DISCUSSION

A. Origin of reduced moment of Yb

The low-temperature magnetic moment of Yb is found to be $1.6\,\mu_B$, a value significantly smaller than $4.5\,\mu_B$ for a free Yb [44]. In h-$YbFeO_3$, Yb is surrounded by seven oxygen atoms, approximately corresponding to C_{3v} symmetry. Analysis using double groups indicates that the $4f_{7/2}$ states are split by the crystal field into four levels: $3E_{1/2} + E_{3/2}$ (see Appendix B), where $E_{1/2}$ and $E_{3/2}$ are both two-dimensional [44]. The energy scale of the crystal-field splitting is typically a few meV to a few tens meV [26–28], which cannot be resolved in the XAS spectra. This crystal-field splitting means that, at low temperature, only the low-lying level (ground state) is populated and contributes to the magnetization. The occupation of the low-lying level, in turn, leads to the reduced value of μ_{Yb}, and it is the reason for the temperature-dependent magnetic moments and magnetic anisotropy observed previously in rare-earth-containing oxides [28,30].

B. Possible spin reorientation and magnetization compensation

One can calculate the temperature dependence of Yb magnetization using Eq. (2). As shown in Fig. 6(a), the result (with $\mu_{\mathrm{Yb}} = 1.6\,\mu_B$, $H = 19$ kOe, and $H_{\mathrm{Yb}} = 17$ kOe) is compared with the measured values. The measured and the calculated magnetization match well below 70 K, suggesting that the mean-field theory can describe the temperature dependence of M_{Yb} too. The fact that the mean-field theory can describe both the magnetic field (Sec. III C 2) and the temperature dependence of M_{Yb} indicates its validity in analyzing the magnetic properties of h-$YbFeO_3$.

On the other hand, at about 80 K, the calculated value is much larger than the measured value, suggesting a reduction of H_{Yb} at higher temperature. To reveal the temperature dependence of H_{Yb}, we calculated H_{Yb} from the measured magnetization value using Eq. (3) (with $\mu_{\mathrm{Yb}} = 1.6\,\mu_B$, $H = 19$ kOe); the result is displayed in Fig. 6(a), inset. Clearly, a sign change of H_{Yb} occurs at about 80 K, indicating a possible realignment between the magnetization M_{Yb} and M_{Fe}, which is discussed below.

In principle, the alignment between M_{Yb} and M_{Fe} is determined by the minimization of total energy,

$$E_{\mathrm{tot}} = -\tfrac{1}{2\mu_0}\chi_{\mathrm{Yb}}(\mu_0 H + \Gamma_{\mathrm{YbFe}} M_{\mathrm{Fe}})^2 - \mu_0 M_{\mathrm{Fe}} H,$$

or the maximization of the total magnetization,

$$M_{\mathrm{tot}} = M_{\mathrm{Fe}}\left(1 + \frac{\chi_{\mathrm{Yb}}\Gamma_{\mathrm{YbFe}}}{\mu_0}\right) + \chi_{\mathrm{Yb}} H.$$

Here the external field H is along the c axis, and M_{Fe} may point either along or opposite to H, corresponding to the positive and negative signs, respectively.

Because $\Gamma_{\mathrm{YbFe}} < 0$ and $\chi_{\mathrm{Yb}} = \frac{\mu_{\mathrm{Yb}}^2 \mu_0}{3k_B T}$ (see Sec. III C 3), the sign of $1 + \frac{\chi_{\mathrm{Yb}}\Gamma_{\mathrm{YbFe}}}{\mu_0}$ is expected to change with temperature, possibly causing the reversal of the direction of the magnetization M_{Fe}:

(i) At low temperature, $1 + \frac{\chi_{\mathrm{Yb}}\Gamma_{\mathrm{YbFe}}}{\mu_0} < 0$. In this case, $M_{\mathrm{Fe}} < 0$ (M_{Fe} antiparallel to H) is more favorable for maximizing M_{tot}; this means the exchange field $H_{\mathrm{Yb}} = \frac{\Gamma_{\mathrm{YbFe}} M_{\mathrm{Fe}}}{\mu_0} > 0$ (parallel to the external field).

(ii) When temperature is increased and $1 + \frac{\chi_{\mathrm{Yb}}\Gamma_{\mathrm{YbFe}}}{\mu_0} > 0$ is satisfied, $M_{\mathrm{Fe}} > 0$ (M_{Fe} parallel to H) is more favorable. In this case, one has the exchange field $H_{\mathrm{Yb}} = \frac{\Gamma_{\mathrm{YbFe}} M_{\mathrm{Fe}}}{\mu_0} < 0$ (antiparallel to the external field); this could be the reason that at about 80 K the H_{Yb} becomes negative [Fig. 6(a), inset].

(iii) At the compensation temperature, $1 + \frac{\chi_{\mathrm{Yb}}\Gamma_{\mathrm{YbFe}}}{\mu_0} = 0$. Therefore, $M_{\mathrm{tot}} = \chi_{\mathrm{Yb}} H$, as if M_{Fe} is screened by the part of the Yb moment induced by the exchange field H_{Yb}. The magnetization compensation can be understood as the cancellation of M_{Fe} and M_{Yb} at zero field. According to Fig. 6(a), inset, the compensation temperature appears to be between 70 and 80 K, in fair agreement with the previous estimation [24].

Nonetheless, the magnetization of the Yb is largely a spectator to that of the Fe. The coercivity is the same as that observed for iron, with the essential observation [Fig. 6(b)] that the magnetization does not easily saturate, indicating that much of the magnetization depends on the magnetic susceptibility

and possible alignment of the moments with external magnetic field H and with the magnetization of Fe (Fig. 7).

C. Exchange field on Fe

The exchange field may also have an effect on the Fe, which can be understood by combining Eqs. (1) and (2) to reach

$$x_{\mathrm{Fe}} = \frac{\left[\Gamma_{\mathrm{YbFe}}\mu_{\mathrm{Yb}}L(\frac{\Gamma_{\mathrm{YbFe}}M_{\mathrm{Fe}}\mu_{\mathrm{Yb}}}{k_BT}) + \Gamma_{\mathrm{Fe}}M_{\mathrm{Fe}}\right]M_{\mathrm{Fe,S}}}{k_BT},$$

assuming $H = 0$. Since Fe moments in h-$YbFeO_3$ form a ferromagnetic order, Γ_{Fe} must be positive. Because of the properties of the Langevin function $L(x)$, $\Gamma_{\mathrm{YbFe}}\mu_{\mathrm{Yb}}L(\frac{\Gamma_{\mathrm{YbFe}}M_{\mathrm{Fe}}\mu_{\mathrm{Yb}}}{k_BT})$ is always positive regardless of the sign of Γ_{YbFe}. Therefore, the Yb always enhances the molecular field on the Fe. That said, because in general $\Gamma_{\mathrm{Fe}} \gg |\Gamma_{\mathrm{YbFe}}|$, the effect may not be significant.

D. Comparison between magnetic properties of h-$YbFeO_3$ and h-$LuFeO_3$

Hexagonal $LuFeO_3$ (h-$LuFeO_3$) is the most studied hexagonal rare-earth ferrite. Because Lu^{3+} is nonmagnetic, the magnetic properties of h-$LuFeO_3$ are less complex. By comparing h-$LuFeO_3$ and h-$YbFeO_3$, one may gain insight into the effect of the rare earth on the magnetism.

One dramatic difference between h-$YbFeO_3$ and h-$LuFeO_3$ is in the coercive field of magnetization. For h-$YbFeO_3$ at 18 K, the coercive field is about 4 kOe, which is much smaller than the value 25 kOe for h-$LuFeO_3$ [16]. For both h-$LuFeO_3$ and h-$YbFeO_3$, the magnetization-field loops of Fe have a squared shape, suggesting that the magnetic coercive field is determined by the competition between the magnetic anisotropy energy and the Zeeman energy. Compared with h-$LuFeO_3$, h-$YbFeO_3$ has enhanced magnetization due to the contribution of Yb. Therefore, a much smaller magnetic field is needed in h-$YbFeO_3$ to overcome the magnetic anisotropy, corresponding to a much smaller coercive field.

Another difference between h-$YbFeO_3$ and h-$LuFeO_3$ is in the saturation magnetization of Fe. According to Fig. 7, in h-$YbFeO_3$, $M_{\mathrm{Fe,S}} = 0.05 \pm 0.01\ \mu_B$/f.u., larger than that in h-$LuFeO_3$ ($\approx 0.03\ \mu_B$/f.u.) [16]. We note that previously it was observed in h-$LuFeO_3$ that the magnetization contains a soft component and a hard component, in which only the hard component ($0.018\ \mu_B$/f.u.) is believed to be intrinsic to the weak ferromagnetic ordering, because it disappears above the magnetic ordering temperature [16]. In Fig. 7, there is also one soft (coercive field ≈ 1 kOe) and one hard component (coercive field ≈ 4 kOe). If we only treat the hard component to be intrinsic to the canting of the Fe moment, the weak ferromagnetic moment of Fe in h-$YbFeO_3$ is $0.03 \pm 0.01\ \mu_B$/Fe [Fig. 7(b)], to still larger compared with the value $0.018\ \mu_B$/f.u. in h-$LuFeO_3$ [16]. Due to the size difference of Lu^{3+} and Yb^{3+} [14], the lattice constants of the basal plane of h-$LuFeO_3$ are smaller than that of h-$YbFeO_3$: $a = 5.963$ Å for h-$LuFeO_3$ and $a = 6.021$ Å for h-$YbFeO_3$ [31]. Our recent work suggests that a compressive biaxial strain may reduce the canting of the Fe moments in h-$YbFeO_3$ [50], which is in line with the correlation between the lattice constant and the weak ferromagnetic moment on Fe observed here.

V. CONCLUSION

We have studied the electronic structure and magnetic ordering of h-$YbFeO_3$ (001) thin films on YSZ (111) and on Fe_3O_4(111)/AL_2O_3(001) substrates. The magnetism of Yb in h-$YbFeO_3$ was studied using the element-specific method x-ray magnetic circular dichroism based on x-ray absorption spectroscopy. From the temperature and magnetic-field dependence of the Yb magnetization, we found that the low-temperature Yb magnetic moment is significantly reduced compared with the value of free Yb^{3+} ions, indicating the effect of the crystal field. The exchange field on Yb, generated by the Fe moments, tends to antialign the magnetization of Fe and Yb at low temperature. We also investigated possible valence mixing of Yb and only found an indication of Yb^{2+} at the surface of samples grown in an Ar environment, suggesting an insignificant effect on the bulk magnetism of h-$YbFeO_3$ studied in this work using XMCD. We expect that future work, such as optical spectroscopy on probing Yb crystal-field levels and theoretical calculations on Yb-Fe interaction strength, may provide more insight into the ferrimagnetism of h-$YbFeO_3$.

ACKNOWLEDGMENTS

This project was primarily supported by the National Science Foundation through the Nebraska Materials Research Science and Engineering Center (Grant No. DMR-1420645) and ECCS 1508541. Additional support was provided by the Semiconductor Research Corporation through the Center for Nanoferroic Devices and the SRC-NRI Center under Task ID 2398.001. Work of Bryn Mawr College is supported by National Science Foundation Career Award (Grant No. NSF DMR-1053854). Work at Oak Ridge National Laboratory was supported by the Division of Scientific User Facilities of the Office of Basic Energy Sciences, US Department of Energy. This research used resources of the Advanced Photon Source, a U.S. Department of Energy (DOE) Office of Science User Facility operated for the DOE Office of Science by Argonne National Laboratory under Contract No. DE-AC02-06CH11357. Use of the Advanced Light Source was supported by the U.S. Department of Energy, Office of Science, Office of Basic Energy Sciences under Contract No. DE-AC02-05CH11231. The Canadian Light Source is funded by the Canada Foundation for Innovation, the Natural Sciences and Engineering Research Council of Canada, the National Research Council Canada, the Canadian Institutes of Health Research, the Government of Saskatchewan, Western Economic Diversification Canada, and the University of Saskatchewan. The research was performed in part in the Nebraska Nanoscale Facility: National Nanotechnology Coordinated Infrastructure, and the Nebraska Center for Materials and Nanoscience, which are supported by the National Science Foundation under Award ECCS: 1542182, and the Nebraska Research Initiative.

APPENDIX A: CONVERTING XMCD CONTRAST TO MAGNETIZATION OF YB

The calculation of the magnetization of Yb from the XMCD contrast at the M edge is significantly different from that of $3d$ metals at the L edge (e.g., Fe, Co, and Ni), due to the

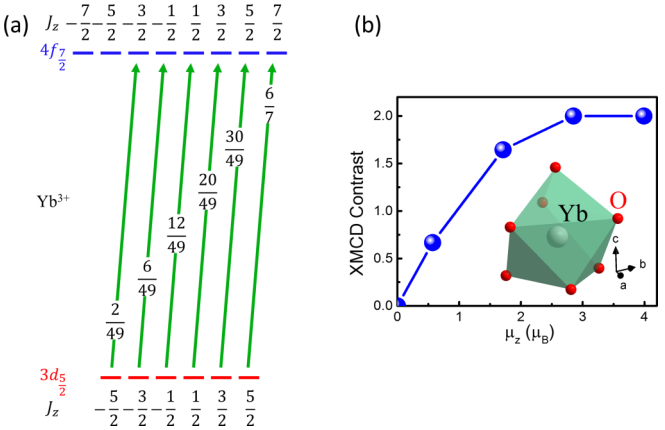

FIG. 9. (a) Transition probability between individual $3d_{5/2}$ and $4f_{7/2}$ states excited by a clockwise polarized x ray. (b) XMCD contrast as a function of μ_z (see the text) calculated assuming a free Yb^{3+} ion. The inset shows the local environment of Yb with a C_{3v} symmetry.

strong spin-orbit coupling in both initial and final states. We hereby present a method based on the XMCD contrast of the excitations from the $3d_{5/2}$ to the individual $4f_{7/2}$ eigenstates $J_z = -7/2$ to $7/2$, where J_z is the projection of total angular moment J on the z axis; all possible $4f_{7/2}$ states are a superposition of these states.

Excited by an x ray polarized clockwise, the transition from one $3d_{5/2}$ state to one $4f_{7/2}$ state needs to satisfy $\Delta J_z = 1$. One can calculate the transition probabilities P between individual states; the nonzero results are displayed in Fig. 9(a). The projection of the magnetic moment of a J_z state on the z direction is $\mu_z = g_B J_z$, where $g = 1.14$ is the Landé g-factor and μ_B is the Bohr magneton. Therefore, one can calculate the XMCD contrast, defined as $\frac{2(P_{J_z} - P_{-J_z})}{P_{J_z} + P_{-J_z}}$, with respect to μ_z, where P_{J_z} (P_{-J_z}) is the transition probability for the final state represented by J_z ($-J_z$); the result is shown in Fig. 9(b). Although for large μ_z the XMCD contrast does not distinguish the $|J_z| = 7/2$ and $5/2$ states, for small μ_z the relation between XMCD contrast and μ_z is approximately linear. The measured XMCD contrast in this work falls in the small μ_z region (all values are less than 0.4). Therefore, we can use the relation in Fig. 9(b) to convert XMCD contrast to magnetization as a fair approximation.

TABLE I. Character table of the double group C_{3v}.

C_{3v}	E	$2C_3$	$3\sigma_v$	RE	$2RC_3$	$3R\sigma_v$
A_1	1	1	1	1	1	1
A_2	1	1	−1	1	1	−1
E	2	−1	0	2	−1	0
$E_{1/2}$	2	1	0	−2	−1	0
$E_{3/2^+}$	1	−1	i	−1	1	$-i$
$E_{3/2^-}$	1	−1	$-i$	−1	1	i
$J = 7/2$	8	1	0	−8	−1	0
$J = 5/2$	6	0	0	−6	0	0

APPENDIX B: GROUP THEORY ANALYSIS OF THE CRYSTAL-FIELD SPLITTING OF YB STATES

In h-$YbFeO_3$, the local environment of Yb has a symmetry that can be described using point group C_{3v} [see Fig. 9(b), inset]. The degenerate electronic states in general are split according to the symmetry of the local environment. Because of the strong spin-orbit coupling, the angular momentum of the $4f$ states takes half-integer $J = \frac{5}{2}$ or $\frac{7}{2}$, the analysis of which requires the double group. Table I shows the character table for the C_{3v} double group, including irreducible representations A_1, A_2, E, $E_{\frac{1}{2}}$, and $E_{\frac{3}{2}}$ ($E_{\frac{3}{2}^+}$ and $E_{\frac{3}{2}^-}$). The characters of the representation with angular momentum $J = \frac{5}{2}$ and $\frac{7}{2}$ are also listed. Using these characters, one can reduce the $J = \frac{5}{2}$ and $\frac{7}{2}$ representations. The results are $J = \frac{5}{2} \rightarrow 2E_{\frac{1}{2}} + E_{3/2\frac{3}{2}}$ and $J = \frac{7}{2} \rightarrow 3E_{\frac{1}{2}} + E_{\frac{3}{2}}$.

[1] R. C. O'Handley, *Modern Magnetic Materials: Principles and Applications* (Wiley, New York, 2000).
[2] R. M. Bozorth, Phys. Rev. Lett. **1**, 362 (1958).
[3] D. Treves, J. Appl. Phys. **36**, 1033 (1965).
[4] D. Treves, Phys. Rev. **125**, 1843 (1962).
[5] R. L. White, J. Appl. Phys. **40**, 1061 (1969).
[6] X. Fabreges, S. Petit, I. Mirebeau, S. Pailhes, L. Pinsard, A. Forget, M. T. Fernandez-Diaz, and F. Porcher, Phys. Rev. Lett. **103**, 067204 (2009).
[7] M. Fiebig, D. Frohlich, K. Kohn, S. Leute, T. Lottermoser, V. V. Pavlov, and R. V. Pisarev, Phys. Rev. Lett. **84**, 5620 (2000).
[8] O. P. Vajk, M. Kenzelmann, J. W. Lynn, S. B. Kim, and S.-W. Cheong, Phys. Rev. Lett. **94**, 087601 (2005).
[9] W. A. Crossley, R. W. Cooper, J. L. Page, and R. P. Van Stapele, Phys. Rev. **181**, 896 (1969).
[10] A. K. Zvezdin and V. M. Matveev, Sov. Phys. JETP **3**, 140 (1972).
[11] V. N. Derkachenko, A. M. Kodomtseva, V. A. Timofeeva, and V. A. Khokhlov, JEPT Lett. **20**, 104 (1974).
[12] E. Magome, C. Moriyoshi, Y. Kuroiwa, A. Masuno, and H. Inoue, Jpn. J. Appl. Phys. **49**, 09ME06 (2010).
[13] W. Wang, J. Zhao, W. Wang, Z. Gai, N. Balke, M. Chi, H. N. Lee, W. Tian, L. Zhu, X. Cheng, D. J. Keavney, J. Yi, T. Z. Ward, P. C. Snijders, H. M. Christen, W. Wu, J. Shen, and X. Xu, Phys. Rev. Lett. **110**, 237601 (2013).
[14] X. Xu and W. Wang, Mod. Phys. Lett. B **28**, 1430008 (2014).
[15] C. J. Fennie and K. M. Rabe, Phys. Rev. B **72**, 100103 (2005).
[16] J. A. Moyer, R. Misra, J. A. Mundy, C. M. Brooks, J. T. Heron, D. A. Muller, D. G. Schlom, and P. Schiffer, APL Mater. **2**, 012106 (2014).
[17] S. M. Disseler, J. A. Borchers, C. M. Brooks, J. A. Mundy, J. A. Moyer, D. A. Hillsberry, E. L. Thies, D. A. Tenne, J. Heron, M. E. Holtz, J. D. Clarkson, G. M. Stiehl, P. Schiffer, D. A. Muller, D. G. Schlom, and W. D. Ratcliff, Phys. Rev. Lett. **114**, 217602 (2015).
[18] H. Das, A. L. Wysocki, Y. Geng, W. Wu, and C. J. Fennie, Nat. Commun. **5**, 2998 (2014).

[19] H. Wang, I. V. Solovyev, W. Wang, X. Wang, P. J. Ryan, D. J. Keavney, J.-W. Kim, T. Z. Ward, L. Zhu, J. Shen, X. M. Cheng, L. He, X. Xu, and X. Wu, Phys. Rev. B **90**, 014436 (2014).
[20] S. Cao, X. Zhang, T. R. Paudel, K. Sinha, X. Wang, X. Jiang, W. Wang, S. Brutsche, J. Wang, P. J. Ryan, J.-W. Kim, X. Cheng, E. Y. Tsymbal, P. A. Dowben, and X. Xu, J. Phys.: Condens. Matter **28**, 156001 (2016).
[21] J. A. Mundy, C. M. Brooks, M. E. Holtz, J. A. Moyer, H. Das, A. F. Rbola, J. T. Heron, J. D. Clarkson, S. M. Disseler, Z. Liu, A. Farhan, R. Held, R. Hovden, E. Padgett, Q. Mao, H. Paik, R. Misra, L. F. Kourkoutis, E. Arenholz, A. Scholl, J. A. Borchers, W. D. Ratcliff, R. Ramesh, C. J. Fennie, P. Schiffer, D. A. Muller, and D. G. Schlom, Nature (London) **537**, 523 (2016).
[22] N. A. Spaldin, S. W. Cheong, and R. Ramesh, Phys. Today **63**(10), 38 (2010).
[23] H. Iida, T. Koizumi, Y. Uesu, K. Kohn, N. Ikeda, S. Mori, R. Haumont, P.-E. Janolin, J.-M. Kiat, M. Fukunaga, and Y. Noda, J. Phys. Soc. Jpn. **81**, 024719 (2012).
[24] Y. K. Jeong, J. Lee, S. Ahn, S.-W. Song, H. M. Jang, H. Choi, and J. F. Scott, J. Am. Chem. Soc. **134**, 1450 (2012).
[25] G. Huber, ECS Trans. **25**, 287 (2009).
[26] R. K. Tamrakar, D. P. Bisen, and N. Brahme, Infr. Phys. Technol. **68**, 92 (2015).
[27] P. Haumesser, E. Antic-fidancev, P. Porcher, B. Viana, and R. Gaume, J. Alloys Compd. **341**, 160 (2002).
[28] X. S. Xu, T. V. Brinzari, S. McGill, H. D. Zhou, C. R. Wiebe, and J. L. Musfeldt, Phys. Rev. Lett. **103**, 267402 (2009).
[29] D. L. Wood, L. M. Holmes, and J. P. Remeika, Phys. Rev. **185**, 689 (1969).
[30] I. Mikami, J. Phys. Soc. Jpn. **34**, 338 (1973).
[31] X. Zhang, Y. Yin, S. Yang, Z. Yang, and X. Xu, J. Phys.: Condens. Matter **29**, 164001 (2017).
[32] S. Cao, T. R. Paudel, K. Sinha, X. Jiang, W. Wang, E. Y. Tsymbal, X. Xu, and P. A. Dowben, J. Phys.: Condens. Matter **27**, 175004 (2015).
[33] W. Wang, H. Wang, X. Xu, L. Zhu, L. He, E. Wills, X. Cheng, D. J. Keavney, J. Shen, X. Wu, and X. Xu, Appl. Phys. Lett. **101**, 241907 (2012).
[34] S. Cao, X. Zhang, K. Sinha, W. Wang, J. Wang, P. A. Dowben, and X. Xu, Appl. Phys. Lett. **108**, 202903 (2016).
[35] J. A. Bearden, Rev. Mod. Phys. **39**, 78 (1967).
[36] N. W. Ashcroft and N. D. Mermin, *Solid State Physics* (Holt, Rinehart and Winston, New York, 1976).
[37] J. Stohr and H. C. Siegmann, *Magnetism from Fundamentals to Nanoscale Dynamics* (Springer, Berlin, 2006).
[38] J. Stohr and H. Konig, Phys. Rev. Lett. **75**, 3748 (1995).
[39] P. Carra, B. T. Thole, M. Altarelli, and X. Wang, Phys. Rev. Lett. **70**, 694 (1993).
[40] K. P. Belov, A. M. Kadomtseva, and R. Z. Levitin, Sov. Phys. JETP **20**, 291 (1965).
[41] K. P. Belov and S. A. Nikitin, Izv. Akad. Nauk SSSR, Ser. Fiz. **34**, 957 (1970).
[42] K. P. Belov and S. A. Nikitin, Sov. Phys. JETP **31**, 505 (1970).
[43] K. P. Belov, A. M. Kadomtseva, N. M. Kovtun, V. N. Derkachenko, V. N. Melov, and V. A. Khokhlov, Phys. Status Solidi **36**, 415 (1976).
[44] M. S. Dresselhaus, G. Dresselhaus, and A. Jorio, *Group Theory Application to the Physics of Condensed Matter* (Springer-Verlag, Berlin, 2007).
[45] R. P. Gupta and S. K. Sen, Phys. Rev. B **12**, 15 (1975).
[46] R. P. Gupta and S. K. Sen, Phys. Rev. B **10**, 71 (1974).
[47] S. Tanuma, T. Shiratori, T. Kimura, K. Goto, S. Ichimura, and C. J. Powell, Surf. Interf. Anal. **37**, 833 (2005).
[48] M. P. Seah and W. A. Dench, Surf. Interf. Anal. **1**, 2 (1979).
[49] Y. Ohno, J. Electron Spectrosc. Relat. Phenom. **165**, 1 (2008).
[50] K. Sinha, Y. Zhang, X. Jiang, H. Wang, X. Wang, X. Zhang, P. J. Ryan, J.-W. Kim, J. Bowlan, D. A. Yarotski, Y. Li, A. D. DiChiara, X. Cheng, X. Wu, and X. Xu, Phys. Rev. B **95**, 094110 (2017).